Chem Biol Drug Des 2013; **82:** 669–684

Research Article

Synthesis and 3D-QSAR Analysis of 2-Chloroquinoline Derivatives as *$H_{37}RV$ MTB* Inhibitors

Ranjan C. Khunt[1],*, Vijay M. Khedkar[2] and Evans C. Coutinho[2]

[1]*Department of Chemistry, Saurashtra University, Rajkot, 360005, India*
[2]*Department of Pharmaceutical Chemistry, Bombay College of Pharmacy, Kalina, Santacruz (E), Mumbai, 400 098, India*
**Corresponding author: Dr. Ranjan C. Khunt, drrckhunt12@yahoo.com*

Frequency of *tuberculosis* is progressively increasing worldwide. New emerging strains of bacilli that are emerging are resistant to the currently available drugs which make this issue more alarming. In this regard, a series of substituted quinolinyl chalcones, quinolinyl pyrimidines, and pyridines were synthesized and evaluated for their antitubercular activity *in vitro* against *Mycobacterium tuberculosis $H_{37}RV$*. To establish the role of the 2-chloroquinoline nucleus as a pharmacophoric group and study its influence on the antimycobacterial activity, a 3D-QSAR study based on CoMFA and CoMSIA was undertaken on this set of 2-chloroquinoline derivatives. Statistically significant models that are able to well correlate the antimycobacterial activity with the chemical structures of the 2-chloroquinolines have been developed. The contour maps resulting from the best CoMFA and CoMSIA models were used to identify the structural features relevant to the biological activity in this series of analogs. Further analysis of these interaction-field contour maps also showed a high level of internal consistency. The information obtained from the field 3-D contour maps may be fruitfully utilized in the design of more potent 2-chloroquinoline-based analogs as potential antitubercular candidates.

Key words: 3D-QSAR, antitubercular activity, chloroquinolines

Received 26 September 2012, revised 3 May 2013 and accepted for publication 28 May 2013

Tuberculosis is caused by several species of mycobacteria, including *Mycobacterium tuberculosis, M. bovis, M. africanum, M. microti, M. avium, and M. leprae* that are intracellular, gram-positive, non-motile, and rod-shaped obligate aerobic pathogens of higher vertebrates (1,2). *Tuberculosis* is an infectious pulmonary disease infecting 8–10 million people globally and causing 3 million deaths every year according to a World Health Organization report (3). Owing to the rapid spread of mycobacterium strains resistant to all first-line antitubercular drugs. such as isoniazid, rifampicin, and ethionamide, and due to the toxicity of second-line drugs, such as ethionamide, aminosalicylic acid, cycloserine, amikacin, kanamycin, and capreomycin, the discovery of new antitubercular agents with improved activity, lower toxicity, broader spectrum, and safer therapeutic profiles is a pressing need (4). The distribution of *tuberculosis* is not uniform across the globe. About 80% of the population in many Asian and African countries test positive in the tuberculin test, while only 5–10% of the US population test positive (5). Globally, 9.2 million new cases and 1.7 million deaths from TB were reported in the year 2006, of which 0.7 million cases and 0.2 million deaths were of HIV-positive people. Among the infected individuals approximately 8 million develop active TB and almost 2 million of these die from this deadly disease. Each year, 95% of new TB cases appear in developing countries (6).

New antitubercular drug regimens are clearly needed to reduce the time required for a durable cure and to treat the ever expanding problem of drug- and multidrug-resistant (MDR) *M. tuberculosis* strains (7).

Despite the efforts of agencies such as WHO; the Global Fund for HIV, TB, and Malaria; and the Gates Foundation which have galvanized multilateral support and initiated public–private partnerships to increase resources to combat this disease of poverty, only seven candidate TB drugs from five different chemical classes are undergoing clinical trials till very recently, these are the fluoroquinolones gatifloxacin and moxifloxacin, a diarylquinoline (TMC207), the nitroimidazoles-OPC67683 and PA824, a pyrrole (LL3858) and an ethylenediamine (SQ109) (8). The need to develop less toxic and more potent compounds against *tuberculosis* has led to the discovery of diarylquinolines that target the mycobacterial F1F0 proton ATP synthase, a new drug target in mycobacteria. Among diarylquinolines, a modified form of diarylquinoline R207910 has been identified as a promising anti-TB drug with *in vitro* activity against *M. smegmatis* (MIC of 0.003 μg/mL) and *M. tuberculosis* (MIC of 0.030 μg/mL) and potent activity against MDR-TB strains (9). It has been reported that C6-substituted pyrimidine derivatives display antitubercular activity (10–14). Pyridines and pyrimidines have also been identified with antitubercular activity and can

 doi: 10.1111/cbdd.12178

be developed as new structural classes of antitubercular agents. Among the pyridines, *N*-alkyl-1,2-dihydro-2-thioxo-3-pyridine carbothioamides have been recognized as a novel class of compounds with good antitubercular activity. Two compounds in this series have an MIC of 0.50 μg/mL (15). Within the pyrimidine group, 2,4-diaminopyrimidines have been identified with IC_{50} of 0.0058 μM and a safety index >600 (16). The most effective analogs show more than 97% inhibition of mycobacterium at a concentration of 2.50 μg/mL and this series was examined in detail by QSAR analysis (17). Thus, this structural class holds great hope for development of new and effective antitubercular agents.

Chalcones have been associated with a wide variety of pharmacological activity and also act as a synthon for preparing new heterocycles (18). Keeping in mind the biomedical applications and in continuation of our previous study, (a)we envisioned the development of a novel series of quinoline derivatives incorporating the pyrimidine in a single molecular framework with a potential spectrum of bioresponses. The antitubercular activity of these compounds against *M. tuberculosis H37Rv strain* was studied using the radiometric BACTEC and broth dilution assay methods. The current work describes the synthesis of a series of 2-chloroquinoline derivatives with encouraging antimycobacterial activity against *M. tuberculosis* $H_{37}Rv$.

To deduce a correlation between structure and biological activity of these 2-chloroquinoline derivatives as antitubercular agents, a 3D-QSAR study employing comparative molecular field analysis (CoMFA) (19,20) and comparative molecular similarity indices analysis (CoMSIA) (21–23) was performed. The structural variations in the molecular fields at particular regions in the space were investigated and the resulting 3D-QSAR models could provide useful indicators for further design of new drug candidates for *tuberculosis*.

Methods and Materials

Melting points were determined in open capillary tubes and are uncorrected. Thin layer chromatography (TLC) was performed on Silica gel G (Merck TLC Plate, Darmstadt, Germany) with the solvent system ethyl acetate: hexane (3:7, v/v); iodine chamber was used for visualization of the TLC spots. ^{1}H NMR was determined in $CDCl_3$ solution on a Bruker DPX 300 MHz spectrometer. ^{13}C NMR (75 and 125 MHz) spectra were registered on a Bruker DPX 300 and ARX 500 at 25 °C in $CDCl_3$. IR spectra were recorded on a Shimadzu 8400 spectrometer in KBr disks. Elemental analysis was carried out on a Carlo Erba 1108 analyzer. The starting material quinoline was prepared using Vilsmeier-Haack synthesis.

Synthesis of 3-(aryl)-1-phenyl-1H-pyrazole-4-carbaldehydes (1)

Synthesis of 3-(aryl)-1-phenyl-1*H*-pyrazole-4-carbaldehydes was achieved by reported method (18).

General method for preparation of 2-chloro-3-(1-arylprop-2-en-1-one-3-yl)-6-fluoro/bromoquinoline (2a–m)

To a solution of 2-chloro-6-fluoro/bromo-quinoline-3-carboxaldehyde (0.01 mol) and substituted acetophenone (0.01 mol) in ethanol (25 mL), 40% NaOH solution was added till the reaction mixture became basic. The reaction mixture was stirred for 24 h. The content was poured onto crushed ice and neutralized. The isolated product was crystallized from ethanol.

2-chloro-3-(1-(3-Nitro)-phenyl-prop-2-en-1-one-3-yl)-6-fluoroquinoline (2a)

Yield 65%, mp 120–121 °C; R_f 0.66; IR (KBr): 3065, 3010, 1668, 1630, 1610, 1585, 1491, 1150, 850, 735 per cm. ^{1}H NMR (300 MHz, $CDCl_3$) δ (ppm): 6.70–7.80 (m, 11H, vinyl + Ar–H), 7.83(d, 1H, J = 15.8 Hz, vinyl proton), 8.12 (t, 1H, J = 8.00 Hz, quinoline), 8.30 (s, 1H, NH), 8.85 (s, 1H, quinoline). ^{13}C NMR ($CDCl_3$) δ (ppm): 109.8, 116.2, 120.0, 126.0, 127.4, 128.1, 130.2, 131.0, 141.0, 143.2, 144.7, 160.0, 191.0. MS m/z: 356 (M^+), 358 (M^{+2}). Anal. Calcd. for $C_{18}H_{10}ClFN_2O_3$: C, 51.77%; H, 2.41%; N, 6.71%. Found: C, 51.67%; H, 2.35%; N, 6.65%.

2-chloro-3-(1-(3,4-dichloro)phenyl-prop-2-en-1-one-3-yl)-6-fluoroquinoline (2b)

Yield 61%, mp 70–72 °C; R_f 0.60; IR (KBr): 3067, 3015, 1670, 1628, 1615, 1580, 1492, 1150, 740, 670 per cm. ^{1}H NMR (300 MHz, $CDCl_3$) δ (ppm): 7.32–7.80 (m, 6H, vinyl + Ar–H), 7.84 (d, 1H, J = 15.8 Hz, vinyl proton), 8.03 (t, 1H, J = 8.00 Hz, quinoline), 8.80 (s, 1H, quinoline). ^{13}C NMR ($CDCl_3$) δ (ppm): 109.7, 116.2, 120.8, 127.1, 129.9, 130.2, 131.6, 135.0, 136.5, 145.2, 148.7. MS m/z: 378.0 (M^+), 380.0 (M^{+2}). Anal. Calcd. for $C_{18}H_9NOCl_3F$: C, 56.80%; H, 2.38%; N, 3.68%. Found: C, 56.72%; H, 2.26%; N, 3.56%.

2-chloro-3-(1-(4-ethoxy)-phenyl-prop-2-en-1-one-3-yl)-6-fluoroquinoline (2c)

Yield 55%, mp 66–68 °C; R_f 0.58; IR (KBr): 3015, 2975, 1670, 1628, 1610, 1590, 1450, 1250, 1075, 740, 650 per cm. ^{1}H NMR (300 MHz, $CDCl_3$) δ (ppm): 1.5 (t, 3H, J = 6.98 Hz, -CH_3), 4.0 (q, 2H, J = 6.96 Hz, -CH_2), 6.96–7.70 (m, 7H, vinyl + Ar–H), 7.85 (d, 1H, J = 15.8 Hz, vinyl proton), 8.12 (t, 1H, J = 8.00 Hz, quinoline), 8.80 (s, 1H, quinoline). ^{13}C NMR ($CDCl_3$) δ (ppm): 14.8, 63.5, 114.8, 129.5, 130.5, 135.6, 146.6, 149.8, 161.8, 164.5, 190.1. MS m/z: 353.0.0 (M^+), 355.0 (M^{+2}). Anal. Calcd. for $C_{20}H_{15}NO_2ClF$: C, 67.52%.; H, 4.25%.; N, 3.94%. Found: C, 67.44%; H, 4.18%; N, 3.86%.

2-chloro-3-(1-(2-thienyl)-prop-2-en-1-one-3-yl)-6-fluoroquinoline (2d)

Yield 58%, mp 144–146 °C; R_f 0.54; IR (KBr): 3020, 1665, 1630, 1600, 1585, 1475, 742, 635 per cm. ^{1}H NMR

(300 MHz, $CDCl_3$) δ (ppm): 7.06–7.65 (m, 8H, vinyl + Ar–H), 7.62 (d, 1H, J = 15.7 Hz, vinyl proton), 8.15 (t, 1H, J = 8.20 Hz, quinoline), 8.79 (s, 1H, quinoline). ^{13}C NMR ($CDCl_3$) δ (ppm): 109.8, 120.4, 128.5, 129.4, 130.7, 131.0, 135.2, 137.2, 139.4, 141.2, 149.8, 161.3, 180.1. MS m/z: 315.0 (M^+), 317.0 (M^{+2}). Anal. Calcd. for $C_{17}H_{11}NOClFS$: C, 60.48%; H, 2.85%; N, 4.41%. Found: C, 60.36%; H, 2.73%; N, 4.32%.

2-chloro-3-(1-(4-fluoro)-phenyl-prop-2-en-1-one-3-yl)-6-fluoroquinoline (2e)

Yield 61%, mp 130–132 °C; R_f 0.48; IR (KBr): 3031, 3080, 1670, 1628, 1616, 1580, 1450, 735, 651 per cm. ^1H NMR (300 MHz, $CDCl_3$) δ (ppm): 7.16–7.79 (m, 7H, vinyl + Ar–H), 7.90 (d, 1H, J = 15.8 Hz,vinyl proton), 8.18 (t, 1H, J = 8.00 Hz, quinoline), 8.85 (s, 1H, quinoline). ^{13}C NMR ($CDCl_3$) δ (ppm): 110.8, 116.8, 121.4, 127.6, 129.2, 130.7, 132.5, 135.4, 136.7, 142.4, 143.3, 149.7, 161.4, 165.9, 190.1. MS m/z: 327.0 (M^+), 329.0 (M^{+2}). Anal. Calcd. for $C_{18}H_{10}NOClF_2$: C, 65.57%; H, 3.06%; N, 4.25%. Found: C, 65.43%; H, 2.96%; N, 4.15%.

2-chloro-3-(1-(4-bromo)-phenyl-prop-2-en-1-one-3-yl)-6-fluoroquinoline (2f)

Yield 62%, mp 134–136 °C; R_f 0.58; IR (KBr): 3110, 3080, 1668, 1628, 1600, 1585, 1450, 781, 685 per cm. ^1H NMR (300 MHz, $CDCl_3$) δ (ppm): 7.32–7.70 (m, 7H, vinyl + Ar–H), 7.92 (d, 1H, J = 15.5 Hz, vinyl proton), 8.20 (t, 1H, J = 8.12 Hz, quinoline), 8.80 (s, 1H, quinoline). ^{13}C NMR ($CDCl_3$) δ (ppm): 111.0, 119.8, 128.7, 129.9, 131.5, 133.5, 134.5, 136.8, 138.4, 143.7, 145.6, 150.7, 161.2, 190.7. MS m/z: 388.0 (M^+), 390.0 (M^{+2}). Anal. Calcd. for $C_{18}H_{10}NOClFBr$: C, 55.34%; H, 2.58%; N, 3.59%. Found: C, 55.22%; H, 2.47%; N, 3.45%.

2-chloro-3-(1-(3,4-dichloro)phenyl-prop-2-en-1-one-3-yl)-6-bromoquinoline (2g)

Yield 59%, mp 240–242 °C; R_f 0.55; IR (KBr): 3150, 3030, 1672, 1630, 1598, 1550, 1450, 781, 741 per cm. ^1H NMR (300 MHz, $CDCl_3$) δ (ppm): 7.40–7.91 (m, 7H, vinyl + Ar–H), 8.01 (t, 1H, J = 8.12 Hz, quinoline), 8.87 (s, 1H, quinoline). ^{13}C NMR ($CDCl_3$) δ (ppm): 122.7, 124.8, 129.7, 132.4, 136.8, 138.9, 139.8, 147.4, 148.2, 151.0, 191.0. MS m/z: 439.0 (M^+), 441.0 (M^{+2}). Anal. Calcd. for $C_{18}H_9NOCl_3Br$: C, 48.96%; H, 2.05%; N, 3.17%. Found: C, 48.84%; H, 1.98%; N, 3.02%.

2-chloro-3-(1-(4-fluoro)phenyl-prop-2-en-1-one-3-yl)-6-bromoquinoline (2h)

Yield 54%, mp 82–84 °C; R_f 0.61; IR (KBr): 3100, 3025, 1667, 1630, 1615, 1585, 1480, 771, 735, 681 per cm. ^1H NMR (300 MHz, $CDCl_3$) δ (ppm): 7.16–7.85 (m, 7H, vinyl + Ar–H), 7.94(d, 1H, J = 15.8 Hz, vinyl proton), 8.35 (d, 1H, J = 8.52 Hz, quinoline), 8.83 (s, 1H, quinoline). ^{13}C NMR ($CDCl_3$) δ (ppm): 118.9, 121.2, 124.7, 128.5, 129.5, 131.8, 135.6, 137.4, 147.7, 148.9, 151.2, 169.8, 189.7. MS m/z: 388.0 (M^+), 390.0 (M^{+2}). Anal. Calcd. for $C_{18}H_{10}NOClBrF$: C, 55.34%; H, 2.58%; N, 3.59%. Found: C, 55.28%; H, 2.45%; N, 3.48%.

2-chloro-3-(1-(4-amino)phenyl-prop-2-en-1-one-3-yl)-6-bromoquinoline (2i)

Yield 55%, mp 118–120 °C; R_f 0.56; IR (KBr): 3400–3200, 3080, 3000, 1664, 1601, 1585, 1490, 1250, 780, 735 per cm. ^1H NMR (300 MHz, $CDCl_3$) δ (ppm): 4.01 (broad, 2H, $-NH_2$), 6.80–7.85 (m, 7H, vinyl + Ar–H), 7.85(d, 1H, J = 15.65 Hz, vinyl proton), 8.05 (d, 1H, J = 7.95 Hz, quinoline), 8.80 (s, 1H, quinoline). ^{13}C NMR ($CDCl_3$) δ (ppm): 118.7, 121.3, 128.7, 129.3, 131.5, 135.6, 136.7, 148.2, 149.4, 158.2, 190.3. MS m/z: 385.0 (M^+), 387.0 (M^{+2}). Anal. Calcd. for $C_{18}H_{12}N_2OCl_2Br$: C, 55.77%; H, 3.12%; N, 7.23%. Found: C, 55.64%; H, 3.01%; N, 7.16%.

2-chloro-3-(1-(2-amino)phenyl-prop-2-en-1-one-3-yl)-6-bromoquinoline (2j)

Yield 59%, mp 88–90 °C; R_f 0.58; IR (KBr): 3350–3250, 3070, 3010, 1660, 1628, 1604, 1590, 1450, 1220, 779, 740 per cm. ^1H NMR (300 MHz, $CDCl_3$) δ (ppm): 3.98 (broad, 2H, $-NH_2$), 7.10–7.75 (m, 8H, vinyl + Ar–H), 8.30 (d, 1H, J = 7.80 Hz, quinoline), 8.82 (s, 1H, quinoline). ^{13}C NMR ($CDCl_3$) δ (ppm): 116.5, 118.5, 121.8, 125.7, 127.2, 129.6, 134.4, 138.6, 141.2, 148.9, 149.4, 150.2, 190.5 MS m/z: 385.0 (M^+), 387.0 (M^{+2}). Anal. Calcd. for $C_{18}H_{12}N_2OClBr$: C, 55.77%; H, 3.12%; N, 7.23%. Found: C, 55.63%; H, 3.05%; N, 7.13%.

2-chloro-3-(1-(2-indene-1-one-3-yl)-6-bromoquinoline (2k)

Yield 44%, mp 143–145 °C; R_f 0.62; IR (KBr): 3140, 3010, 2975, 1662, 1630, 1598, 1491, 781, 740 per cm. ^1H NMR (300 MHz, $CDCl_3$) δ (ppm): 4.10 (s, 2H, CH_2), 7.01–7.75 (m, 7H, vinyl + Ar–H), 8.30 (d, 1H, J = 7.80 Hz, quinoline), 8.82 (s, 1H, quinoline). ^{13}C NMR ($CDCl_3$) δ (ppm): 121.8, 125.7, 127.2, 129.6, 134.4, 138.6, 141.2, 148.9, 149.4, 150.2, 190.5. MS m/z: 382.0 (M^+), 384.0 (M^{+2}). Anal. Calcd. for $C_{19}H_{11}NOClBr$: C, 61.11%; H, 3.66%; N, 3.39%. Found: C, 60.98%; H, 3.58%; N, 3.27%.

2-chloro-3-(1-(4-ethoxyphenyl)prop-2-en-1-one-3-yl)-6-bromoquinoline (2l)

Yield 58%, mp 170–172 °C; R_f 0.49; IR (KBr): 3115, 3030, 2980, 1673, 1600, 1585, 1493, 1250, 1075, 780, 731 per cm. ^1H NMR (300 MHz, $CDCl_3$) δ (ppm):1.20 (t, 3H, J = 6.90 Hz, CH_3), 4.02 (q, 2H, J = 6.98 Hz, CH_2), 6.96–7.75 (m, 7H, vinyl + Ar–H), 7.85 (d, 1H, J = 15.8 Hz, vinyl), 8.15 (d, 1H, J = 7.80 Hz, quinoline), 8.80 (s, 1H,

quinoline). ^{13}C NMR ($CDCl_3$) δ (ppm): 15.8, 63.2, 116.7, 121.4, 123.2, 128.7, 130.1, 131.7, 132.3, 135.8, 147.6, 148.9, 150.4, 162.3, 191.8. MS m/z: 414.0 (M^+), 416.0 (M^{+2}). Anal. Calcd. for $C_{20}H_{15}NO_2ClBr$: C, 57.65%; H, 3.63%; N, 3.36%. Found: C, 57.58%; H, 3.59%; N, 3.31%.

2-chloro-3-(1-(3-nitrophenyl)prop-2-en-1-one-3-yl)-6-bromoquinoline (2m)

Yield 52%, mp 154–156 °C; R_f 0.51; IR (KBr): 3110, 3010, 1660, 1628 1601, 1585, 1450, 1250, 1075, 850, 780, 735 per cm. ^{1}H NMR (300 MHz, $CDCl_3$) δ (ppm): 7.75–8.47 (m, 9H, vinyl + Ar–H, quinoline), 8.85 (s, 1H, quinoline). ^{13}C NMR ($CDCl_3$) δ (ppm): 121.8, 124.8, 129.0, 134.0, 136.0, 139.8, 149.8, 151.7, 153.6, 189.2. MS m/z: 415.0 (M^+), 417.0 (M^{+2}). Anal. Calcd. for $C_{18}H_{10}N_2O_3ClBr$: C, 51.77%; H, 2.41%; N, 6.71%. Found: C, 51.65%; H, 2.35%; N, 6.62%.

General method for preparation of 2-chloro-3-(2-amino-3-cyano-4-arylpyridin-6-yl)-6-fluoro/bromoquinoline (3a–g)

An equimolar mixture of 2-chloro-3-(1-arylprop-2-en-1-one-3-yl)-6-fluoro/bromoquinoline (compound **II**) and malononitrile with ammonium acetate (0.08 M) in 30 mL ethanol was heated under reflux for 6 h. The reaction mixture was poured onto crushed ice, and the product was crystallized from ethanol.

2-chloro-3-(2-amino-3-cyano-4-(4-ethoxyphenyl) pyridin-6-yl)-6-fluoroquinoline (3a)

Yield 58%, mp 144–146 °C; R_f 0.55; IR (KBr): 3400–3200, 3020, 2960, 2148, 1630, 1600, 1550, 1250, 1100, 1075, 740, 648 per cm. ^{1}H NMR (300 MHz, $CDCl_3$) δ (ppm): 1.33 (t, 3H, J = 6.98 Hz, $-CH_3$), 3.99 (q, 2H, J = 6.96 Hz, $-CH_2$), 4.05 (broad, 2H, $-NH_2$), 6.83–8.03 (m, 8H, Ar–H + quinoline + pyridine), 9.01 (s, 1H, quinoline). ^{13}C NMR ($CDCl_3$) δ (ppm): 14.9, 64.7, 87.0, 109.2, 115.0, 116.8, 121.2, 127.1, 128.7, 138.7, 139.5, 141.2, 152.0, 158.3, 159.4, 160.9. MS m/z: 402.0 (M^+), 404.0 (M^{+2}). Anal. Calcd. for $C_{23}H_{16}N_4OClF$: C, 65.25%; H, 3.49%; N, 13.14%. Found: C, 65.10%; H, 3.36%; N, 13.02%.

2-chloro-3-(2-amino-3-cyano-4-(2,4-dichlorophenyl)-pyridin-6-yl)-6-fluoroquinoline (3b)

Yield 56%, mp 129–131 °C; R_f 0.52; IR (KBr): 3410–3250, 3015, 2150, 1628, 1592, 1100, 735, 680 per cm. ^{1}H NMR (300 MHz, $CDCl_3$) δ (ppm): 3.92 (broad, 2H, $-NH_2$), 7.21–7.47 (m, 6H, Ar–H + quinoline + pyridine), 8.15 (t, 1H, J = 8.00 Hz, quinoline), 8.85 (s, 1H, quinoline). ^{13}C NMR ($CDCl_3$) δ (ppm): 89.2, 19.5, 110.1, 115.7, 121.0, 121.7, 127.5, 130.5, 135.8, 137.0, 145.7, 151.8, 157.6, 158.9, 160.9.0 MS m/z: 439.00 (M^+), 441.0 (M^{+2}). Anal. Calcd. for $C_{21}H_{10}N_4Cl_3F$: C, 56.85%; H, 2.27%; N, 12.63%. Found: C, 56.78%; H, 2.19%; N, 12.54%.

2-chloro-3-(2-amino-3-cyano-4-(4-flouorophenyl)-pyridin-6-yl)-6-fluoroquinoline (3c)

Yield 61%, mp 269–270 °C; 0.60; R_f 0.60; IR (KBr): 3410–3250, 3080, 2120, 1628, 1550, 1498, 1100, 740, 645 per cm. ^{1}HNMR (300 MHz, $CDCl_3$) δ (ppm): 4.01 (broad, 2H, $-NH_2$), 7.03–7.49 (m, 7H, Ar–H + quinoline + pyridine), 8.09 (t, 1H, J = 8.00 Hz, quinoline), 8.95 (s, 1H, quinoline). ^{13}C NMR ($CDCl_3$) δ (ppm): 88.7, 110.5, 115.8, 117.1, 121.0 125.8, 127.2, 130.0, 135.5, 137.8, 145.5, 151.0, 155.8, 157.4, 161.8, 163. MS m/z: 390.0 (M^+), 392.0 (M^{+2}). Anal. Calcd. for $C_{21}H_{11}N_4ClF_2$: C, 64.21%; H, 2.82%; N, 14.26%. Found: C, 64.13%; H, 2.75%; N, 14.18%.

2-chloro-3-(2-amino-3-cyano-4-(2-theinyl)-pyridin-6-yl)-6-fluoroquinoline (3d)

Yield 55%, mp 110–55 °C; R_f 0.58; IR (KBr): 3415–3215, 3120, 2150, 1628, 1575, 1498, 1100, 740, 680 per cm. ^{1}H NMR (300 MHz, $CDCl_3$) δ (ppm): 4.02 (broad, 2H,-NH_2), 7.01–7.47 (m, 6H, Ar–H + quinoline + pyridine), 8.15 (t, 1H, J = 8.00 Hz, quinoline), 8.90 (s, 1H, quinoline). ^{13}C NMR ($CDCl_3$) δ (ppm): 90.2, 110.2, 121.8, 127.6, 130.2, 133.4, 135.8, 139.7, 142.0, 147.9, 151.8, 157.9, 161.0. MS m/z: 378.00 (M^+), 380.0 (M^{+2}). Anal. Calcd. for $C_{19}H_{10}N_4ClFS$: C, 59.92%; H, 2.65%; N, 14.71%. Found: C, 59.81%; H, 2.58%; N, 14.63%.

2-chloro-3-(2-amino-3-cyano-4-(4-bromophenyl)-pyridin-6-yl)-6-fluoroquinoline (3e)

Yield 53%, mp 159–161 °C; R_f 0.53; IR (KBr): 3400–3200, 3031, 2130, 1630, 1575, 1498, 1100, 780, 735, 645 per cm.^{1}H NMR (300 MHz, $CDCl_3$) δ (ppm): 3.98(broad, 2H, $-NH_2$), 7.32–7.49 (m, 7H, Ar–H + quinoline + pyridine), 8.15 (t, 1H, J = 8.10 Hz, quinoline), 8.89 (s, 1H, quinoline). ^{13}C NMR ($CDCl_3$) δ (ppm): 89.7, 109.5, 110.2, 117.7, 121.8, 125.4, 128.2, 130.1, 132.3, 135.5, 136.8, 145.5, 151.1, 155.8, 159.7, 161.0. MS m/z: 449.0 (M^+), 451.0 (M^{+2}). Anal. Calcd. for $C_{21}H_{11}N_4ClFBr$: C, 55.59%; H, 2.44%; N, 12.35%. Found: C, 55.42%; H, 2.36%; N, 12.26%.

2-chloro-3-(2-amino-3-cyano-4-(3-nitrophenyl)-pyridin-6-yl)-6-bromoquinoline (3f)

Yield 57%, mp 154–156 °C; R_f 0.49; IR (KBr): 3400–3200, 3080, 2150, 1628, 1575, 1580, 1497, 1132, 780, 735 per cm. ^{1}H NMR (300 MHz, $CDCl_3$) δ (ppm): 4.02 (broad, 2H, $-NH_2$), 7.47-7.91 (m, 7H, Ar–H), 8.15 (t, 1H, J = 8.00 Hz, quinoline), 8.85 (s, 1H, quinoline). ^{13}C NMR ($CDCl_3$) δ (ppm): 89.4, 110.0, 115.8, 121.2, 125.7, 129.0, 131.1, 132.3, 135.5, 136.8, 147.5, 151.8, 155.7, 158.2, 162.0. MS m/z: 478.0 (M^+), 480.0 (M^{+2}). Anal. Calcd. for $C_{21}H_{11}N_5ClFBr$: C, 52.47%; H, 2.31%; N, 14.57%. Found: C, 52.38%; H, 2.25%; N, 14.46%.

2-chloro-3-(2-amino-3-cyano-4-(3, 4-dichlorophenyl)-pyridin-6-yl)-6- bromoquinoline (3g)

Yield 50%, mp 159–161 °C; R_f 0.55; IR (KBr): 3450–3200, 3030, 2150, 1628, 1595, 1580, 1498, 1150, 780, 741 per cm. ^{1}H NMR (300 MHz, $CDCl_3$) δ (ppm): 4.01 (broad, 2H, -NH_2), 7.27-7.81 (m, 6H, Ar–H + quinoline + pyridine), 8.12 (d, 1H, J = 8.07 Hz, quinoline), 8.85 (s, 1H, quinoline). ^{13}C NMR ($CDCl_3$) δ (ppm): 89.0, 110.3, 115.0, 122.0, 126.1, 128.0, 133.8, 134.5, 138.8, 149.5, 151.8, 154.7, 156.2, 162.0. MS m/z: 499.0 (M^+), 501.0 (M^{+2}). Anal. Calcd. for $C_{21}H_{10}N_4Cl_3Br$: C, 49.99%; H, 2.00%; N, 11.10%. Found: C, 49.85%; H, 1.87%; N, 11.01%.

General preparation of 2-chloro-3-(2-amino-4-phenyl-pyrimidin–6-yl)-6-fluoroquinoline (4a–h)

An equimolar mixture of 2-chloro-3-(1-aryl-prop-2-en-1-on-3yl)-6-fluoro/bromoquinoline (2), guanidine hydrochloride was irradiated with microwave radiation at 480 power for 10 min in the presence of catalytically amount of potassium carbonate. Then, the product was isolated with ethanol and crystallized it.

2-chloro-3-(2-amino-4-(4-ethoxyphenyl)pyrimidin-6-yl)-6-fluoroquinoline (4a)

Yield 60%, mp 279–281 °C; R_f 0.62; IR (KBr): 3430–3200, 3020, 2980, 1628, 1600, 1575, 1580, 1498, 1250, 1100, 1075, 741, 680 per cm. ^{1}H NMR (300 MHz, $CDCl_3$) δ (ppm): 1.35 (t, 3H, -CH_3), 3.98 (q, 2H, -CH_2), 4.01 (broad, 2H, -NH_2), 6.98–7.48 (m, 7H, Ar–H + quinoline + pyrimidine), 8.12 (t, 1H, J = 8.10 Hz, quinoline), 8.85 (s, 1H, Quinoline). ^{13}C NMR ($CDCl_3$) δ (ppm): 14.6, 64.7, 93.7, 110.8, 114.7, 121.2, 123.5, 126.8, 127.9, 130.2, 132.5, 135.8, 142.7, 150.0, 158.7, 161.8, 163.9, 164.7. MS m/z: 392.0 (M^+), 394.0 (M^{+2}). Anal. Calcd. for $C_{21}H_{16}N_4ClFO$: C, 63.88%; H, 4.08%; N, 14.19%. Found: C, 63.76%; H, 3.97%; N, 14.03%.

2-chloro-3-(2-amino-4-(3,4-dichlorophenyl) pyrimidin-6-yl)-6-fluoroquinoline (4b)

Yield 59%, mp 180–181 °C; R_f 0.52; IR (KBr): 3410–3215, 3030, 1630, 1600, 1556, 1498, 1115, 741, 680 per cm. ^{1}H NMR (300 MHz, $CDCl_3$) δ (ppm): 4.05(broad, 2H, -NH_2), 6.96–7.43 (m, 6H, Ar–H + quinoline + pyrimidine), 8.12 (t, 1H, J = 8.20 Hz, quinoline), 8.85 (s, 1H, quinoline). ^{13}C NMR ($CDCl_3$) δ (ppm): 93.4, 109.9, 121.0, 127.5, 130.3, 132.5, 135.8, 142.3, 149.3, 160.9, 162.8, 164.0. MS m/z: 415.0 (M^+), 417.0 (M^{+2}). Anal. Calcd. for $C_{19}H_{10}N_4Cl_3F$: C, 54.38%; H, 2.40%; N, 13.35%. Found: C, C, 54.24%; H, 2.27%; N, 13.27%.

2-chloro-3-(2-amino-4-(4-fluorophenyl)pyrimidin-6-yl)-6-fluoroquinoline (4c)

Yield 62%, mp 114–116 °C; R_f 0.62; IR (KBr): 3415–3250, 3028, 1628, 1601, 1558, 1497, 1110, 735, 680 per cm. ^{1}H NMR (300 MHz, $CDCl_3$) δ (ppm): 4.05 (broad, 2H, -NH_2), 7.10–7.46 (m, 7H, Ar–H + quinoline + pyrimidine), 8.15 (t, 1H, J = 8.00 Hz, quinoline), 8.83 (s, 1H, quinoline). ^{13}C NMR ($CDCl_3$) δ (ppm): 94.1, 109.5, 116.4, 121.0, 128.5, 129.9, 130.7, 132.5, 135.8, 144.3, 150.0, 158.2, 161.8, 163.2, 164.7. MS m/z: 366.0 (M^+), 368.0 (M^{+2}). Anal. Calcd. for $C_{19}H_{11}N_4ClF_2$: C, 61.88%; H, 3.01%; N, 15.19%. Found: C, 61.75%; H, 2.84%; N, 15.05%.

2-chloro-3-(2-amino-4-(2-thienyl)- pyrimidin-6-yl)-6-fluoroquinoline (4d)

Yield 55%, mp 284–286 °C; R_f 0.63; IR (KBr): 3415–3200, 1630, 1610, 1598, 1498, 1120, 735, 680, 670 per cm. ^{1}H NMR (300 MHz, $CDCl_3$) δ (ppm): 4.10 (broad, 2H, NH_2), 7.10–7.41 (m, 6H, Ar–H + quinoline + pyrimidine), 8.12 (t, 1H, J = 8.00 Hz, quinoline), 8.92 (s, 1H, quinoline). ^{13}C NMR ($CDCl_3$) δ (ppm): 92.8, 109.0, 121.0, 127.6, 130.3, 131.8, 135.7, 140.2, 143.7, 149.7, 157.9, 160.2, 162.8. MS m/z (%):354.0 (M^+), 356.0 (M^{+2}). Anal. Calcd. for $C_{17}H_{10}N_4ClFS$: C, 57.23%; H, 2.82%; N, 15.70%. Found: C, 57.08%; H, 2.75%; N, 15.66%.

2-chloro-3-(2-amino-4-(9H-indeno[2,1-a]pyrimidin-6-yl)-6-fluoroquinoline (4e)

Yield 54%, mp 183–185 °C; R_f 0.56; IR (KBr): 3410-3210, 1629, 1608, 1597, 1495, 1110, 780, 741, 635 per cm. ^{1}H NMR (300 MHz, $CDCl_3$) δ (ppm): 3.81 (s, 2H, indonyl), 4.05 (broad, 2H, -NH_2), 7.12–7.49 (m, 6H, Ar–H + quinoline + pyrimidine), 8.18 (d, 1H, J = 8.03 Hz, quinoline), 8.93 (s, 1H, quinoline). ^{13}C NMR ($CDCl_3$) δ (ppm): 94.1, 110.0, 121.0, 123.7, 128.2, 129.7, 130.3, 135.8, 160.9, 162.8. MS m/z: 427.0 (M^+), 429.0 (M^{+2}). Anal. Calcd. for $C_{20}H_{12}N_4ClFBr$: C, 53.11%; H, 2.58%; N, 13.04%. Found: C, 53.01%; H, 2.46%; N, 12.87%.

2-chloro-3-(2-amino-4-(4-bromophenyl)pyrimidin-6-yl)-6-bromoquinoline (4f)

Yield 42%, mp 164–166 °C; R_f 0.58; IR (KBr): 3450–3210, 1630, 1611, 1598, 1497, 1140, 780, 741, 635 per cm. ^{1}H NMR (300 MHz, $CDCl_3$) δ (ppm): 4.10 (broad, 2H, -NH_2), 7.15–7.91 (m, 7H, Ar–H + quinoline + pyrimidine), 8.18 (d, 1H, J = 8.15 Hz, quinoline), 8.80 (s, 1H, quinoline). ^{13}C NMR ($CDCl_3$) δ (ppm): 29.9, 115.8, 121.8, 125.7, 127.9, 129.9, 131.2, 135.8, 138.9, 145.8, 151.2, 160.0, 161.2, 170.0. MS m/z: 421.0 (M^+), 423.0 (M^{+2}). Anal. Calcd. for $C_{19}H_{11}N_4ClBr_2$: C, 58.49%; H, 3.57%; N, 12.40%. Found: C, 58.36%; H, 3.41%; N, 12.28%.

2-chloro-3-(2-amino-4-(3, 4 dichlorophenyl) pyrimidin-6-yl)-6-bromoquinoline (4g)

Yield 53%, mp 164–166 °C; R_f 0.54; IR (KBr): 3450–3200, 1628, 1610, 1598, 1497, 1150, 780, 741 per cm. ^{1}H NMR (300 MHz, $CDCl_3$) δ (ppm): 4.10 (broad, 2H, -NH_2), 7.01–7.91 (m, 6H, Ar–H + quinoline + pyrimidine), 8.18 (d,

1H, J = 8.10 Hz, quinoline), 8.85 (s, 1H, quinoline). ^{13}C NMR ($CDCl_3$) δ (ppm): 93.4, 121.8, 127.0, 128.8, 129.1, 130.8, 133.9, 134.6, 135.3, 145.8, 151.2, 155.4, 162.3, 164.0. MS m/z (%):479.0 (M^+), 480.0 (M^{+2}). Anal. Calcd. for $C_{19}H_{10}N_4Cl_3Br$: C, 47.49%; H, 2.10%; N, 11.66%. Found: C, 47.38%; H, 2.02%; N, 11.58%.

2-chloro-3-(2-amino-4-(3-nitrophenyl)-3, 4-dihydropyrimidin-1H-6-yl)-6-bromoquinoline (4h)

Yield 50%, mp 189–191 °C; R_f 0.52; IR (KBr): 3410–3200, 1635, 1600, 1590, 1497, 1140, 780, 741 per cm. ^{1}H NMR (300 MHz, $CDCl_3$) δ (ppm): 4.12 (broad, 2H, -NH_2), 7.10 (s, 1H, pyrimidine) 7.58–7.80 (m, 6H, Ar–H + quinoline), 8.15 (d, 1H, J = 8.57 Hz, quinoline), 8.85 (s, 1H, quinoline). ^{13}C NMR ($CDCl_3$) δ (ppm): 93.7, 121.3, 122.0, 129.9, 131.8, 134.6, 136.8, 144.7, 149.7, 150.1, 158.7, 164.3, 166.0. MS m/z (%):454.0 (M^+), 456.0 (M^{+2}). Anal. Calcd. for $C_{19}H_{11}N_5O_2ClBr$: C, 49.97%; H, 2.43%; N, 15.34%. Found: C, 49.82%; H, 2.32%; N, 15.23%.

Biological activity

All compounds discussed in the previous section were screened for their antitubercular activity. The activity was carried out against *Mycobacterium tuberculosis* H37Rv, (ATCC-27294) strain using the broth dilution assay method (24,25). The antitubercular activity is presented in Table 1. The antitubercular activity was measured (by TAACF, USA *Tuberculosis* Antimicrobial Acquisition and Coordinating Facility) for all the compounds at a fixed concentration of 6.25 μg/mL. Following this, only those compounds showing more than 90% inhibition at this concentration were tested further for measuring the MIC values; these are quoted in the Table 1. For the remaining molecules because no MIC values were measured, we have used an alternate strategy that has been well published and accepted (12,13,26) to transform the activity data that could be used in 3D-QSAR as the dependent variable. The activity data were transformed as follows:

$$\text{Biological activity} = -\log c + \text{logit}$$

where c is the molar concentration = concentration (μg/mL) × 0.001/(molecular weight) and logit = log[% inhibition/(100−% inhibition)].

Computational details

The 3D-QSAR studies (CoMFA and CoMSIA) were performed with the QSAR module integrated in *Sybyl 7.1*[a] molecular modeling software package from Sybyl.Sybyl, Version 7.1, Tripos Associate Inc., St. Louis, MO, USA, running on a Pentium IV computer under the Centos WS 4.8 as OS.

Ligand preparation

The choice of the template molecule and its conformation are of utmost importance in the development of a 3D-QSAR model. In this investigation, molecule **3e** (Table 1) was selected as the template molecule because it is the most active compound in the data set. Because the bioactive conformation of these 2-chloroquinoline analogs is not known, the lowest energy conformation of **3e** was searched using a simulated annealing approach and used as a template to generate the conformation of the remaining molecules. The ligand geometries were optimized by energy minimization using the Powell gradient method, with the Gasteiger–Hückel charges for the atoms and the standard Tripos force field, to a convergence gradient of 0.001 kcal/mol/Å.

Molecular alignment

The spatial alignment of molecules under study is one of the most crucial and determining factors in obtaining a reliable model. Molecular alignment was performed using the database alignment in *Sybyl* with the atom-fit superimposition technique. The lowest energy conformation of the molecules was used to align on the template molecule **3e**. The atoms selected for molecular alignment were based on the common substructure of the molecules, due to its effectiveness and easy implementation.

Training and test sets

The data set was segregated into a training set for generating 3D-QSAR models and a test set (27) for validating the models. This was carried out on the basis of chemical and biological diversity using similarity search techniques *viz.* D-optimal design, Tanimoto similarity coefficient, and the Euclidian distance matrix criteria defined in *Cerius2*.[b] The selection of the training and test sets was carried out such that the test-set compounds had structural diversity and a range of biological activities similar to that of the training set. This approach grouped 10 compounds into the test set leaving other 18 compounds to form the training set. The test set was used to evaluate the predictive power of the CoMFA and CoMSIA models. The structures and biological activity of the compounds in the training and test sets are listed in Table 1.

CoMFA and CoMSIA setup

After alignment of the molecules in the data set, CoMFA and CoMSIA studies were carried with the QSAR option in *Sybyl*. CoMFA steric and electrostatic interaction fields were calculated at each intersection point of a 3D cubic lattice with a regularly spaced grid of 2 Å, extending to 4 Å beyond the aligned molecules in all directions. The van der Waals potentials and Coulombic terms representing the steric and electrostatic fields, respectively, were calculated using the Tripos force field with a distance dependent dielectric. A sp3 hybridized carbon atom with a charge of +1 served as the probe atom to calculate steric and electrostatic fields. The CoMFA steric and electrostatic fields thus generated were scaled by the CoMFA-STD

Table 1: The experimental and predicted activity values for the molecules

Molecule ID	Structure	*Mycobacterium tuberculosis H37* % inhibition (6.25 μg)	Observed activity	Predicted activity (CoMFA)	Predicted activity (CoMSIA) (SHD)
2a	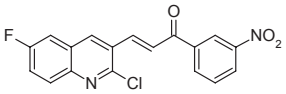	9%	2.88	2.82	2.82
2b	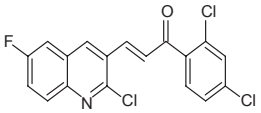	13%	2.96	2.91	2.80
2c	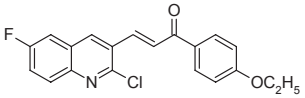	13%	5.75	4.21	4.48
2d	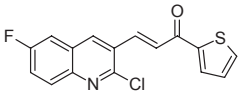	21%	3.13	3.18	3.22
2e	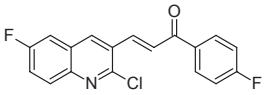	7%	2.60	2.60	2.70
2f	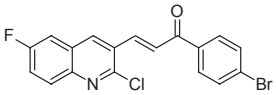	98% (5.0)	5.49	3.84	4.85
2g	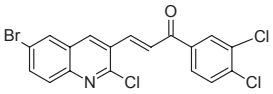	5%	2.57	2.55	2.62
2h	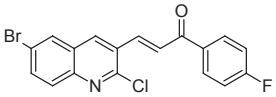	99% (6.25)	5.79	4.35	4.04
2i	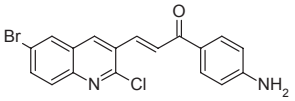	13%	2.97	3.06	2.96
2j	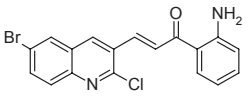	6%	2.60	2.63	2.55
2k	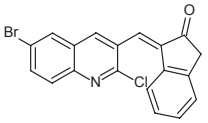	41%	3.66	3.53	3.92
2l	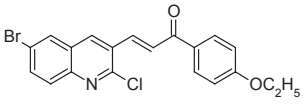	19%	3.19	3.19	3.27

Table 1: continued

Molecule ID	Structure	*Mycobacterium tuberculosis H37* % inhibition (6.25 μg)	Observed activity	Predicted activity (CoMFA)	Predicted activity (CoMSIA) (SHD)
2m	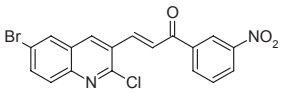	11%	2.92	2.88	2.89
3a	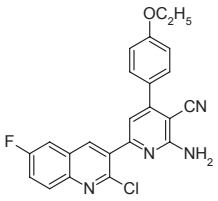	24%	3.31	3.37	3.71
3b	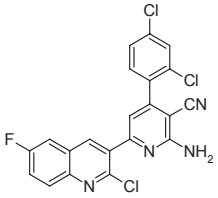	8%	2.79	2.71	3.44
3c	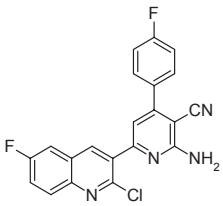	99% (4.5)	5.79	5.86	5.32
3d	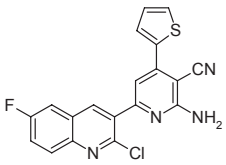	21%	3.21	3.27	3.76
3e	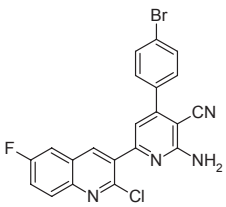	99% (6.25)	5.86	5.75	5.97
3f	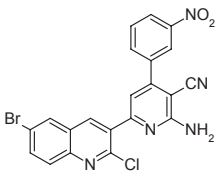	6%	2.69	2.95	3.71
3g	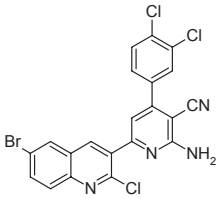	3%	2.40	2.48	3.58

Table 1: continued

Molecule ID	Structure	*Mycobacterium tuberculosis H37* % inhibition (6.25 μg)	Observed activity	Predicted activity (CoMFA)	Predicted activity (CoMSIA) (SHD)
4a	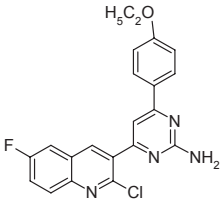	97% (5)	5.31	5.32	5.35
4b	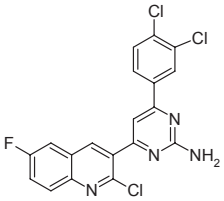	12%	2.96	3.10	3.07
4c	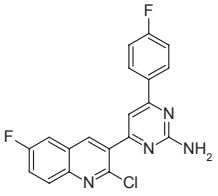	36%	3.52	3.52	3.48
4d	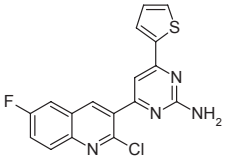	9%	2.75	2.72	2.43
4e	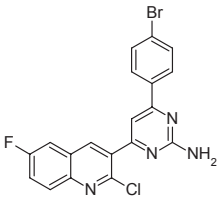	3%	2.33	2.66	3.61
4f	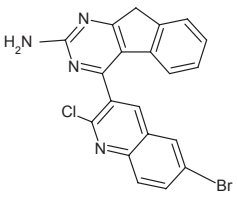	14%	3.07	3.09	3.13

Table 1: continued

Molecule ID	Structure	*Mycobacterium tuberculosis H37* % inhibition (6.25 μg)	Observed activity	Predicted activity (CoMFA)	Predicted activity (CoMSIA) (SHD)
4g	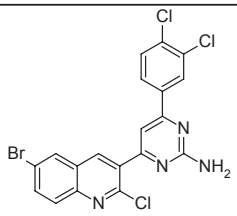	16%	3.17	3.00	3.12
4h	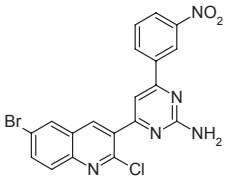	99% (6.25)	5.86	4.65	5.97

method and their energy values were truncated at ±30 kcal/mol.

As an extension to the CoMFA approach which has just two fields, CoMSIA incorporates five different interaction energy fields, namely steric, electrostatic, hydrophobic, hydrogen bond donor, and hydrogen bond acceptor. CoMSIA descriptors were calculated with the same lattice box as that used for the CoMFA calculations, with a grid spacing of 2 Å and a sp3 hybridized carbon atom as the probe with values for the radius as 1.0 Å, charge +1.0, hydrophobicity +1.0, and H-bond properties (donor and acceptor) +1.0. A Gaussian type distance dependence was used between the grid point and each atom in the molecule with a default value of 0.3 as the attenuation factor.

Partial least squares (PLS) (28) regression was used to derive the 3D-QSAR models with the standard implementation in the *Sybyl* package. The CoMFA and CoMSIA descriptors were used as independent variables, while the biological activity data served as the dependent variable. Initial PLS regression analyses were performed in conjunction with the cross-validation (leave-one-out method) (29,30) option to obtain the optimal number of components which were subsequently used in deriving the final CoMFA and CoMSIA models. To avoid over-fitting of data, the number of components corresponding to the highest cross-validated q^2 value and the smallest PRESS value was used. The conventional correlation coefficient r^2 and the standard error of estimate (SEE) were subsequently computed for the final models using the optimal number of components.

To further assess the statistical confidence and robustness of the derived 3D-QSAR models, a 100-cycle bootstrap analysis (31) using the optimum number of components was performed. This procedure involves the generation of multiple new data sets from the original data sets, after random sampling from the original data set. In each run, some molecules may be excluded in the PLS analysis, whereas some others might be included more than once. Also y-scrambling (32) (100-trials) was performed on the chosen 3D-QSAR models to probe the dependence of the model on chance correlations. External predictivity of the models was determined by calculating the r^2_{pred} from a test set of 10 compounds that were not included in the model generation procedure.

The results of the 3D-QSAR studies were visualized as 3D 'coefficient contour maps' (contoured in terms of contribution) generated by interpolation of the pairwise products between the PLS coefficients (coeff) and the standard deviations (stdev) of the corresponding CoMFA and CoMSIA descriptor values. These maps signify those areas in 3D space where variations in steric, electrostatic, and hydrogen bonding features in the molecular structures correlate strongly with corresponding changes in activities.

Results and Discussion

Chemistry

2-Chloroquinoline-3-carbaldehyde has been synthesized by Vilsmeier reaction on *p*-fluoro or bromo substituted acetanilide (Scheme 1). The chalcones (**2a**–**m**) have been synthesized by condensation of compound **1** with different aromatic ketones using the Claisen–Schmidt condensation. The chalcones on cyclization with ammonium acetate and malononitrile or with guanidine hydrochloride furnished cyanopyridines (**3a**–**e**) and aminopyrimidines, respectively (**4a**–**g**). The molecules (**3a**–**m** to **4a**–**g**) (Table 1) were

characterized by ^{1}H NMR, ^{13}C NMR, and mass spectrometry techniques and their purity established by elemental analysis. IR spectra of molecules (**3a**–**m**) show the characteristic band at 2150–2200 per cm for the cyano group and the characteristic band at 3400–3200 per cm for the amino group. ^{1}H NMR spectra are also in agreement with these structures.

Biological activity

The analogs **2h**, **4a**, and **4h** exhibit promising activity and inhibit the growth of mycobacterium to 97%, 98%, and 99%, respectively, at a concentration of 6.25 μg/mL. Analogs **3c** and **3e** were found to be the most active of the series inhibiting the growth of drug-sensitive bacteria to 99% at 4.25 and 6.25 μg/mL concentration, respectively. The remaining analogs of the series produced moderate inhibition in the range of 5–41% (Table 1). A visualizing SAR suggests that R = 4-F-C_6H_5 is more active against Mycobacterium *HRV-37* in case of chalcone and cyanopyridine derivatives.

3D-QSAR studies

The major objective behind CoMFA and CoMSIA analysis is to find features associated with activity within the system. The CoMFA and CoMSIA models based on atom-fit alignment are given in Table 2, which shows that all the statistical indices are in an acceptable domain.

The CoMFA model generated for the 2-chloroquinolines has (r^2_{cv}) of 0.69 and a conventional correlation coefficient (r^2) of 0.99 with a bootstrap correlation coefficient (r^2_{bs}) of 0.98. Also a low standard error of estimate (SEE) of 0.09 with an excellent F value of 384.18 suggests the statistical significance of the derived CoMFA model. These values suggest that the model should be able to predict the activity of compounds outside the training set but within this structural class. Furthermore, a significantly low r^2 of 0.11 obtained for y-scrambling (100 cycles) eliminates the possibility of chance correlation. The contributions of the steric and electrostatic fields are 47% and 53%, respectively. The statistical significance of these models is further supported by the 'fitness plot' which shows the observed versus predicted activity of training and test-set compounds and provides an idea about how well the model was trained and how well it predicts the activity of the external test set (Figures 1A and 2A).

Table 2: Statistical results of the CoMFA and CoMSIA models

	CoMFA	CoMSIA (SHD)
N	18	18
q^2	0.69	0.61
r^2	0.99	0.96
r^2_{pred}	0.64	0.60
r^2_{bs}	0.98	0.97
r^2 *y-scrambling*	0.11	0.15
F	384.18	147.47
SE	0.09	0.12
Field contribution		
Steric	0.47	0.25
Electrostatic	0.53	
Hydrophobic		0.28
H-bond donor		0.47

The CoMSIA analysis was performed using the same structural alignment, PLS protocol, and the training/ test sets as defined in the CoMFA study. Several models were developed considering steric, electrostatic, hydrogen bonding, and hydrophobic fields either separately or in combinations to determine which of the five fields are actually able to explain the structure activity relationships. It was observed that using the steric, hydrogen bond donor, hydrogen bond acceptor, and hydrophobic fields when used independently yielded models with a lower q^2 value. However, the CoMSIA model derived from the combination of steric, hydrophobic, and H-bond donor field produced a model with the highest cross-validated coefficient (q^2) of 0.61, indicating a good predictive capacity with SEE of 0.12 and the F-test value of 147.47. The squared correlation coefficient r^2 of 0.96 with boot strap r^2_{bs} of 0.97 suggests a good internal consistency exists within the underlying data set. Furthermore, a low r^2 of 0.15 obtained by y-scrambling eliminates the possibility of chance correlation. The relationship between experimental and predicted activities for the training/test-set compounds is illustrated in Figures 1B and 2B. The contributions of steric, hydrophobic, and hydrogen bond donor fields to this model are 25%, 28%, and 47%, respectively.

The predictive ability of the 3D-QSAR models was gauged from the r^2_{pred} calculated for each of these models. The predicted r^2 values for the CoMFA and CoMSIA models were found to be 0.64 and 0.60, respectively. These values suggest that models can be used to predict the inhibitory activity of untested compounds.

The major advantage of CoMFA and CoMSIA techniques is that the information contained in these models can be visualized as 3D contour plots which can be fruitfully used to tune molecules to improve their activity. The contour plots were generated as scalar products of coefficients and standard deviation (stdev*coeff), associated with the CoMFA or CoMSIA column. These contour maps indicate regions where differences in steric, electrostatic, hydrophobic, and hydrogen bond fields may affect the biological activity.

The CoMFA steric and electrostatic contour maps obtained from the final non-cross-validated analysis are shown in Figures 3A and 3B, respectively, associated with reference compound, **3e**. Green contours indicate regions where steric bulk is tolerable and can be exploited to improve the activity while yellow contours indicate regions

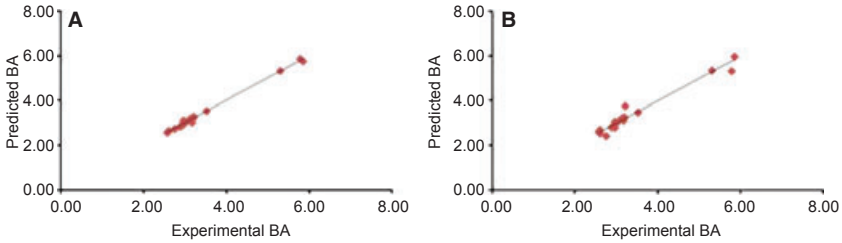

Figure 1: The 'fitness plot' showing the observed vs. predicted activity of training-set compounds for CoMFA (A) and CoMSIA (B) models.

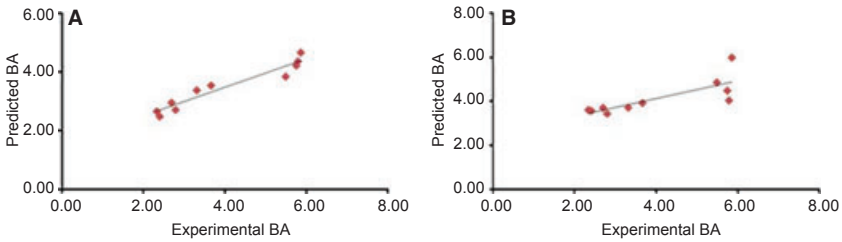

Figure 2: The 'fitness plot' showing the observed vs. predicted activity of test-set compounds for CoMFA (A) and CoMSIA (B) models.

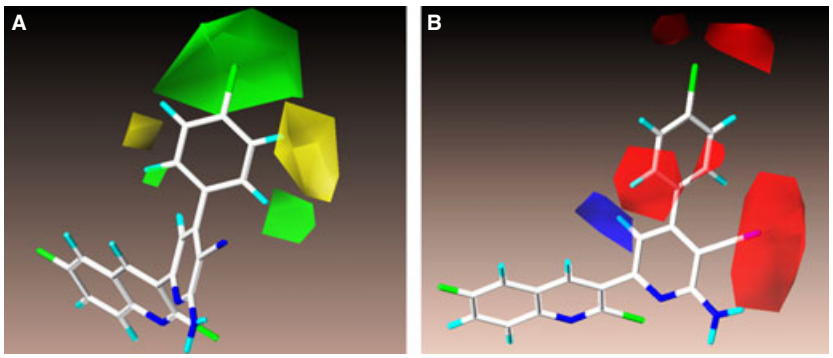

Figure 3: The CoMFA molecular interaction fields around the most active molecule (A) steric contours – favored (green); disfavored (yellow) (B) electrostatic contours – electropositive (blue); electronegative (red).

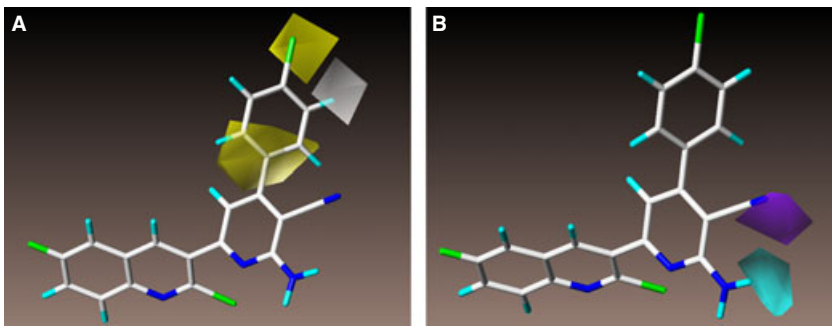

Figure 4: The CoMSIA molecular interaction fields around most active molecule (A) hydrogen bond donor contours – favored (cyan); disfavored (purple) (B) Hydrophobic contours – favored (Yellow); disfavored (white).

where steric bulk is detrimental to the activity. Large green contours are found localized around the *ortho* and *para* positions of ring (D) indicating that the steric bulk is favored in this region. This is consistent with experimental results where compounds **3c**, **3e**, and **4a** with a *para* substituent are more active than those that lack substituent at this position. As regards, compounds **2a**–**2m** which do not have the pyridine ring (C) at the 3rd position of the quinoline nucleus, like **3e**, the substituted aromatic ring present at this position adopts an orientation analogous to the most active compound **3e**. The *para* substituent on the phenyl ring of compounds **2f** and **2h** extends into the green contour and as a result, these compounds are as active as **3e**. Yellow contours are observed around the *meta* position of ring (D) indicating that any steric substituent at this position would greatly reduce the biological activity, suggesting limited bulk tolerance. Less active compounds, as exemplified by **3f**, **3g**, and **4g**, are found with their *meta* substituents oriented in the direction of the yellow contour. Likewise, compounds **2g** and **2m** possessing a *meta* substituent on the phenyl ring also have lower activity.

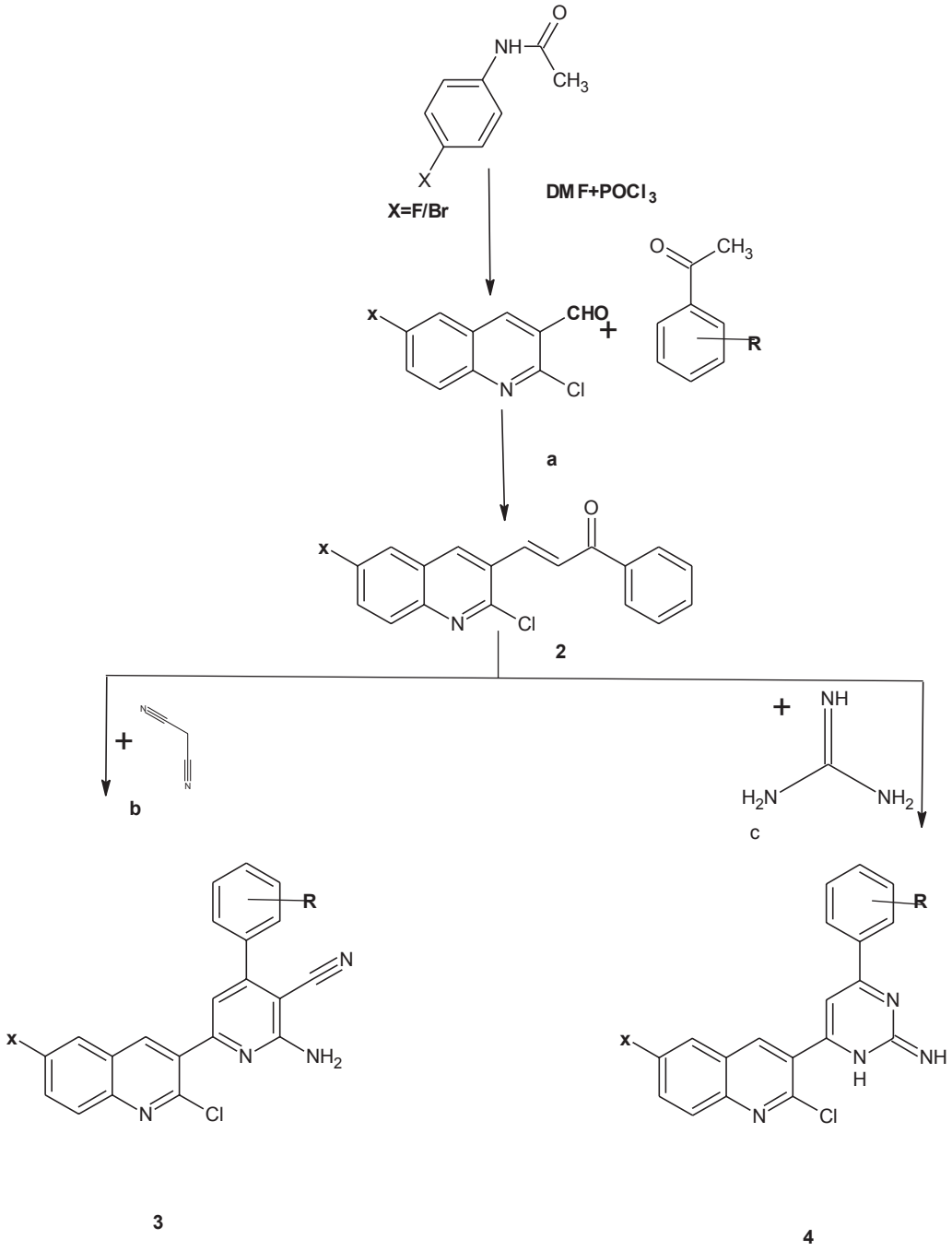

R= 4-OC_2H_5,4-F,4-Br,4-NH_2. 2-NH_2,2,-4,(Cl),3,4(Cl),2-Thenyl : X=F/Br.

Scheme 1: Synthesis of pyridine and pyrimidine; Reagents and condition: (a) 40% NaOH; (b) CH_3COONH_4; (c) K_2CO_3, Microwave irradiation; Reflux..

The electrostatic contour maps of the CoMFA model are characterized by red isopleths near the *para* and *ortho* positions of ring (D) as well as around the cyano substituent of pyridine ring (C). This indicates that increasing electronegativity at these positions should lead to increase in antitubercular activity. This is evident from compounds **3c**, **3e**, and **4a** bearing an electronegative substituent which show good antitubercular activity. Even compounds **2f** and **2h** bearing an electronegative substitution at the *para* position of the phenyl ring display high

activity. A small blue contour is observed around the 5′ position of ring © indicating that a reduction in the electronegativity near this position should lead to increase in activity.

The CoMSIA steric regions are in agreement with the CoMFA steric contours and therefore for the sake of brevity are not discussed again. The hydrophobic map of the CoMSIA model cloaked around the most potent compound **3e** is displayed in Figure 4A. The presence of yellow contour around the *ortho* and *para* positions of ring (D) suggests that occupancy by hydrophobic groups at these sites would favor increase in the activity. Compounds **3c**, **3e**, and **4a** possessing such substituents at these positions display better activity than compounds lacking such substituents. Similarly, compounds **2f** and **2h** with a *para* substituent on the phenyl ring also show higher activity than compounds without a corresponding group. Also a small white contour disfavoring hydrophobic substitution is observed around the *meta* position of ring (D). This is supported by compounds **3f**, **3g**, **4g**, and **4h** with substituents at this position which have poor antitubercular activity. As regards H-bonding, a cyan contour favoring the presence of a hydrogen bond donor functionality is observed around the amino group on the pyridine ring (C) while a purple contour disfavoring the presence of an H-bond donor substituent is observed around the cyano group placed at the 3′ position of the pyridine ring (C) in the most active compound **3e**.

Thus, in the absence of information on the binding mode of these 2-chloroquinoline derivatives, the putative interaction fields obtained from this comparative 3D-QSAR study will be helpful for improving the antitubercular activity in this series of molecules. Considering this fact, a set of new 2-chloroquinoline analogs has been proposed as discussed in the next section which display higher antitubercular activity.

Conclusions

The synthesis and biological evaluation of a series of 2-chloro-3-substitued 6-bromo/fluoroquinolines as antitubercular agents has been discussed. Most importantly, this work validated our initial proposition that pyridine/pyrimidine-substituted quinoline scaffolds would lead to molecules with potent antitubercular activity. 3-Formylquinoline synthesized by the Vilsmeier reaction, on Claisen condensation with substituted acetophenones yielded the chalcones. These chalcones were converted to a variety of 2-chloro-3-substitued-6-bromo/fluoro quinolines which were then screened for antitubercular activity. The study resulted in the identification of compounds **2f**, **2h**, **3c**, **3e**, **4a**, and **4h** as promising inhibitors of *M. tuberculosis*. The q^2 and r^2 values of the CoMFA and CoMSIA models were statistically sound and suggest that all the reported inhibitors would bind to the receptor in an almost similar fashion. While the CoMFA model could point to the importance of steric and electrostatic fields, the CoMSIA model could explain the contribution of hydrophobic and hydrogen bond donor fields as well. CoMFA/CoMSIA models possess good predictive ability as discerned from the result for the external test set and were used to guide the further development of some new 2-chloroquinolines which are predicted with improved activities.

Acknowledgments

RCK thanks the Department of Chemistry, Saurashtra University which is supported by SAP (UGC) for infrastructure facilities and FIST(DST), New Delhi for financial support under the Fast Track Young Scientist Scheme. We also thank Dhanshukh Rajani, Microcare Laboratory, Surat for the antitubercular screening. The computational facilities were jointly provided by the All India Council of Technical Education through grant (F. No. 8022/RID/NPROJ/RPS-5/2003-04), the Department of Science and Technology through their FIST program (SR/FST/LSI-163/2003), Department of Biotechnology (BT/PR11810/BRB/10/690/2009), and the Council of Scientific and Industrial Research (01/23/99/10-EMR-II).

References

1. Asgharzadeh M., Kafil H.S. (2007) Current trends in molecular epidemiology studies of *Mycobacterium tuberculosis*. Biotechnol Mol Biol Rev;2:108–115.
2. Chakraborty A.K. (2004) Epidemiology of *tuberculosis*: current status in India. Indian J Med Res;120:248–276.
3. World Health Organization. (2007) Global *Tuberculosis* Control: Surveillance, Planning, Financing: WHO Report 2008. Geneva, Switzerland: World Health Organization.
4. Scior T., Meneses Morales I., Garces Eisele S.J., Domeyer D., Laufer S. (2002) Antitubercular isoniazid and drug resistance of *Mycobacterium tuberculosis*–a review. Arch Pharm (Weinheim);335:511–525.
5. Iseman M.D. (2002) *Tuberculosis* therapy: past, present and future. Eur Respir J Suppl;36:87s–94s.
6. Ginsberg A.M. (2008) Emerging drugs for active *tuberculosis*. Semin Respir Crit Care Med;29:552–559.
7. Tripathi R.P., Tewari N., Dwivedi N., Tiwari V.K. (2005) Fighting *tuberculosis*: an old disease with new challenges. Med Res Rev;25:93–131.
8. Nikonenko B.V., Protopopova M., Samala R., Einck L., Nacy C.A. (2007) Drug therapy of experimental *tuberculosis* (TB): improved outcome by combining SQ109, a new diamine antibiotic, with existing TB drugs. Antimicrob Agents Chemother;51:1563–1565.

9. Gelber R., Andries K., Paredes R.M.D., Andaya C.E.S., Burgos J. (2009) The diarylquinoline R207910 is bactericidal against *Mycobacterium leprae* in mice at low dose and administered intermittently. Antimicrob Agents Chemother;53:3989.
10. Molina P., Aller E., Lorenzo A., López-Cremades P., Rioja I., Ubeda A., Terencio M.C., Alcaraz M.J. (2001) Solid-phase synthesis and inhibitory effects of some pyrido[1,2-c]pyrimidine derivatives on leukocyte formations and experimental inflammation. J Med Chem; 44:1011–1014.
11. Bhardwaj S.D., Jolly V.S. (1997) Synthesis, anti-HIV and anticancer activities of some new formazans. Asian J Chem;9:48–51.
12. Nayyar A., Monga V., Malde A., Coutinho E., Jain R. (2007) Synthesis, anti-*tuberculosis* activity, and 3D-QSAR study of 4-(adamantan-1-yl)-2-substituted quinolines. Bioorg Med Chem;15:626–640.
13. Nayyar A., Malde A., Jain R., Coutinho E. (2006) 3D-QSAR study of ring-substituted quinoline class of anti-*tuberculosis* agents. Bioorg Med Chem;14:847–856.
14. Nayyar A., Malde A., Coutinho E., Jain R. (2006) Synthesis, anti-*tuberculosis* activity, and 3D-QSAR study of ring-substituted-2/4-quinolinecarbaldehyde derivatives. Bioorg Med Chem;14:7302–7310.
15. Ubiali D., Pagani G., Pregnolato M., Piersimoni C., Pedraz Munoz J.L., Rodriguez Gascon A., Terreni M. (2002) New N-alkyl-1,2-dihydro-2-thioxo-3-pyridinecarbothioamides as antituberculous agents with improved pharmacokinetics. Bioorg Med Chem Lett;12:2541–2544.
16. Rosowsky A., Forsch R.A., Queener S.F. (2002) Inhibition of Pneumocystis carinii, Toxoplasma gondii, and Mycobacterium avium dihydrofolate reductases by 2,4-diamino-5-[2-methoxy-5-(omega-carboxyalkyloxy)benzyl]pyrimidines: marked improvement in potency relative to trimethoprim and species selectivity relative to piritrexim. J Med Chem;45:233–241.
17. Desai B., Sureja D., Naliapara Y., Shah A., Saxena A.K. (2001) Synthesis and QSAR studies of 4-substituted phenyl-2,6-dimethyl-3, 5-bis-N-(substituted phenyl)carbamoyl-1,4-dihydropyridines as potential antitubercular agents. Bioorg Med Chem;9:1993–1998.
18. Khunt R.C., Khedkar V.M., Chawda R.S., Chauhan N.A., Parikh A.R., Coutinho E.C. (2012) Synthesis, antitubercular evaluation and 3D-QSAR study of N-phenyl-3-(4-fluorophenyl)-4-substituted pyrazole derivatives. Bioorg Med Chem Lett;22:666–678.
19. Cramer R.D. III, Patterson D.E., Bunce J.D. (1988) Comparative molecular field analysis (CoMFA). I. effect of shape on binding of steroids to carrier proteins. J Am Chem Soc;110:5959–5967.
20. Cramer R.D. III, Patterson D.E., Bunce J.D. (1989) Recent advances in comparative molecular field analysis (CoMFA). Prog Clin Biol Res;291:161–165.
21. Klebe G., Abraham U., Mietzner T. (1994) Molecular similarity indices in a comparative analysis (CoMSIA) of drug molecules to correlate and predict their biological activity. J Med Chem;37:4130–4146.
22. Klebe G. (1998) Comparative molecular similarity indices analysis: CoMSIA. Perspect Drug Discov Design;12:87–104.
23. Klebe G., Abraham U. (1999) Comparative molecular similarity index analysis (CoMSIA) to study hydrogen-bonding properties and to score combinatorial libraries. J Comput Aided Mol Des;13:1–10.
24. Yajko D.M., Madej J.J., Lancaster M.V., Sanders C.A., Cawthon V.L., Gee B., Babst A., Hadley W.K. (1995) Colorimetric method for determining MICs of antimicrobial agents for *Mycobacterium tuberculosis*. J Clin Microbiol;33:2324–2327.
25. Suling W.J., Seitz L.E., Pathak V., Westbrook L., Barrow E.W., Zywno-Van-Ginkel S., Reynolds R.C., Piper J.R., Barrow W.W. (2000) Antimycobacterial activities of 2,4-diamino-5-deazapteridine derivatives and effects on mycobacterial dihydrofolate reductase. Antimicrob Agents Chemother;44:2784–2793.
26. Manvar A., Malde A., Verma J., Virsodia V., Mishra A., Upadhyay K., Acharya H., Coutinho E., Shah A. (2008) Synthesis, anti-tubercular activity and 3D-QSAR study of coumarin-4-acetic acid benzylidene hydrazides. Eur J Med Chem;43:2395–2403.
27. Golbraikh A., Tropsha A. (2002) Predictive QSAR modeling based on diversity sampling of experimental datasets for the training and test set selection. J Comput Aided Mol Des;16:357–369.
28. Wold S., Johansson E., Cocchi M. (1993) PLS: partial least squares projections to latent structures. In: Kubinyi H., editor. PLS: Partial Least Squares Projections to Latent Structures. Leiden: ESCOM Science Publishers; p. 523–550.
29. Stone M. (1974) Cross-validatory choice and assessment of statistical predictions. J Roy Stat Soc B;36:111–147.
30. Richard D., Cramer R.D. III, Bunce J.D., Patterson D.E., Frank I.E. (1988) Crossvalidation, bootstrapping, and partial least squares compared with multiple regression in conventional QSAR studies. Quant Struct-Act Relat;7:18–25.
31. Shao J. (1996) Bootstrap model selection. J Am Stat Assoc;91:655–665.
32. Rucker C., Rucker G., Meringer M. (2007) y-Randomization and its variants in QSPR/QSAR. J Chem Inf Model;47:2345–2357.

Notes

[a]Sybyl. (2005) Sybyl. In: editor^editors. *Sybyl*. 1699 S Hanley Rd., St. Louis, MO 631444, USA: Tripos Associates Inc.; p.

[b]Accelrys I. (1998) Cerius2. In: editor^editors. *Cerius2*. San Diego, CA, USA; p.

Supporting Information

Additional Supporting Information may be found in the online version of this article:

Figure S1. NMR spectra of compound **2a**.

Figure S2. Expanded NMR spectra of compound **2a**.

Figure S3. NMR spectra of compound **3b**.

Figure S4. NMR spectra of compound **4a**.

Figure S5. Mass spectra of compound **2a**.

Figure S6. Mass spectra of compound **3a**.

Figure S7. Mass spectra of compound **4a**.